INSTRUCTIONAL LABORATORIES AND DEMONSTRATIONS | MAY 01 2025

Coherent diffraction imaging in the undergraduate laboratory

J. Nicholas Porter; David J. Anderson; Julio Escobedo; David D. Allred; Nathan D. Powers; Richard L. Sandberg

Am. J. Phys. 93, 415–421 (2025)
https://doi.org/10.1119/5.0245088

John Essick, *Editor*
Department of Physics, Reed College, Portland, OR 97202

Articles in this section deal with new ideas and techniques for instructional laboratory experiments, for demonstrations, and for equipment that can be used in either. Although these facets of instruction also appear in regular articles, this section is for papers that primarily focus on equipment, materials, and how they are used in instruction. Manuscripts should be submitted using the web-based system that can be accessed via the American Journal of Physics home page, ajp.aapt.org, and will be forwarded to the IL&D editor for consideration.

Coherent diffraction imaging in the undergraduate laboratory

J. Nicholas Porter,[a] David J. Anderson, Julio Escobedo,[b] David D. Allred,[c] Nathan D. Powers,[d] and Richard L. Sandberg[e]
Department of Physics and Astronomy, Brigham Young University, N-284 ESC, Provo, Utah 84604

(Received 23 October 2024; accepted 13 March 2025)

We present an undergraduate optics instructional laboratory designed to teach skills relevant to a broad range of modern scientific and technical careers. In this laboratory project, students image a custom aperture using coherent diffraction imaging, while learning principles and skills related to digital image processing and computational imaging, including multidimensional Fourier analysis, iterative phase retrieval, noise reduction, finite dynamic range, and sampling considerations. After briefly reviewing these imaging principles, we describe the required experimental materials and setup for this project. Our experimental apparatus is both inexpensive and portable, and a software application we developed for interactive data analysis is freely available.
https://doi.org/10.1119/5.0245088

I. INTRODUCTION

Coherent diffraction imaging (CDI) is an indirect imaging method that has seen significant development over the past half-century. It consists of measuring the diffraction pattern produced by an object under coherent illumination, then applying various algorithms to reconstruct the object. Because these algorithms provide a similar function to the objective (image-forming) lens in traditional imaging, CDI is sometimes called a "lensless" imaging technique. The primary application of CDI is in x-ray microscopy, where high photon energies make efficient objective lenses difficult or impossible to manufacture. X-ray CDI has been used to image proteins,[1,2] crystals,[3,4] integrated circuits,[5,6] quantum dots,[7] and more.

In this article, we present an optics instructional laboratory designed for upper-division undergraduate students in which they construct an optical setup and carry out a CDI experiment. While CDI itself occupies a relatively small scientific niche, it involves principles that apply to many other fields such as digital signal processing, computational imaging, and sampling. By applying these principles experimentally, students gain skills and insights that will help prepare them for a wide range of scientific and technical careers. In Sec. II, we briefly review a theoretical diffraction model based on Fourier transforms, a nonconvex optimization algorithm for image reconstructions, and a few practical considerations related to digital imaging. In Sec. III, we then discuss the experimental optical setup and measurements, including the physical apparatus and software resources required. We conclude with some potential ways the laboratory can be expanded into a longer-term project.

The described experiment is intended for second- or third-year undergraduate students familiar with wave mechanics. It is assumed that the students have had some exposure to Fourier transforms, but proficiency with Fourier analysis is not required. However, if Secs. II A and II B are left out, it could potentially be used with younger audiences. While the result would likely be more of a demonstration than a true hands-on lab, it may still be exciting for students to see.

II. COHERENT DIFFRACTION IMAGING

In this section, we discuss a few important principles in CDI. The discussions are necessarily brief, focusing on high-level understanding while omitting many details and applications. Vector quantities are notated in boldface.

A. Fourier diffraction model

To understand how Fourier transforms are related to diffraction and CDI, we start by assuming a uniform, monochromatic plane wave of light is propagating through space with wavelength λ. That light then passes through an "object plane," which modulates the wavefront with some spatially dependent function. For the experiment presented here, the

object plane is an aperture, which blocks any light outside of some finite (not necessarily contiguous) region, such as a set of pinholes in a piece of heavy black paper. The complex-valued light field immediately after the object plane—before any diffraction occurs—is called the *exit wave* ψ, denoted as the red plane in Fig. 1. Assuming that the initial illumination is truly uniform, any spatial variations in the exit wave must have been imparted by the object. In other words, information about the absorptive and refractive properties of the object are encoded into the exit wave.

The light then propagates some distance z to another plane. Wave interference alters the amplitudes and phases as the light propagates, resulting in a new light field Ψ, i.e., the diffraction pattern denoted by the blue plane in Fig. 1. The same information is contained in both the complex exit wave and diffraction pattern, though they often look quite different. The primary goal of CDI is to use the diffraction pattern (which is more easily measured) to obtain the exit wave (which is more easily interpreted).

In the paraxial (small-angle scattering) approximation, the light fields ψ and Ψ are related by the Fresnel equation,[8]

$$\Psi(\mathbf{q}) = -\frac{ike^{ikz}e^{i(k/2z)q^2}}{2\pi z}\int \psi(\mathbf{r})e^{-i(k/2z)(\mathbf{q}\cdot\mathbf{r})}e^{i(k/2z)r^2}\,d\mathbf{r}, \tag{1}$$

where $\mathbf{r}$ is the vector position in the object plane, $\mathbf{q}$ is the vector position in the diffraction plane, and $k = 2\pi/\lambda$ is the wavenumber. If a converging lens is introduced one focal length before the diffraction plane, it can be shown that Eq. (1) takes the form of a Fourier transform,[8,9]

$$\Psi(\mathbf{q}) = -\frac{ike^{ikf}e^{i(k/2f)(1-(d/f))q^2}}{\sqrt{2\pi f}}\mathcal{F}[\psi(\mathbf{r})]_{\mathbf{r}\to(k/f)\mathbf{q}}, \tag{2}$$

where f is both the focal length of the lens and the distance from the lens to the diffraction plane, and $\mathbf{r} \to (k/f)\mathbf{q}$ indicates that the transformed coordinates $\mathbf{q}$ are scaled by the factor k/f. In this arrangement, the lens is called a *Fourier lens*. Because image sensors capture only the intensity of a light field ($I = |\Psi|^2$) and their values are expressed in analog digital units (ADUs), which are not generally calibrated to any absolute units, it is more common in CDI to express the diffraction pattern without the leading constants,

$$|\Psi(\mathbf{q})|^2 \propto |\mathcal{F}[\psi(\mathbf{r})]_{\mathbf{r}\to(k/f)\mathbf{q}}|^2. \tag{3}$$

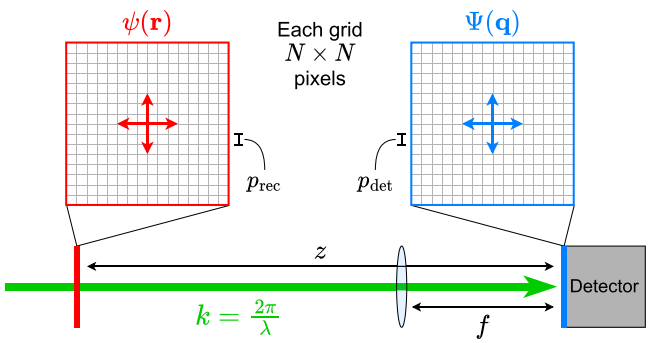

Fig. 1. (Color online) Diagram of key quantities in a diffraction model. Coherent light (green) propagates from left to right with a uniform amplitude and phase. After passing through an object plane (blue), the modified wave field is given by $\psi(\mathbf{r})$. The light then propagates to a detector plane (red), where its amplitude and phase are given by $\Psi(\mathbf{q})$. A lens may be introduced one focal length before the detector plane. Equations (1) and (2) relate the two wave fields without and with the lens, respectively.

Recognizing the connection between diffraction and Fourier transforms can help students gain valuable insight into both topics. For example, it is a natural way to introduce the concept of spatial frequencies. On the other hand, if students lack the required background in Fourier analysis, it may be appropriate to say simply that there is a reversible mathematical operator (the Fourier transform) relating the light profile of the aperture to that of the diffraction pattern. Additional resources on diffraction and Fourier optics can be found in both undergraduate and graduate textbooks.[8,9]

Before moving on, it should be noted that Eq. (1) can take a Fourier-like form *without* a lens by using the Fraunhofer/far-field approximation. While this model is both simpler and more aligned with the assertion of CDI as "lensless," we recommend the lensed version shown here for two practical reasons. First, it can be quickly and easily converted into a traditional imaging apparatus, allowing students to verify their reconstructions. Second, the Fraunhofer approximation is valid only when the propagation distance is large compared to object area divided by wavelength. For the present experiment (area $\sim$1 mm^2, wavelength $\sim$500 nm), this condition would require z to be on the order of several meters. At that distance, the diffraction pattern becomes both too large and too dim to be adequately measured by most image sensors.

B. Phase retrieval

Equation (3) describes a pathologically lossy measurement, since Ψ is a complex-valued field with amplitude and phase, while $|\Psi|$ represents only the amplitude. As shown in Fig. 2, back-propagating a diffraction amplitude numerically with a Fourier transform without the correct phase fails to produce an image of the aperture. This effect is generally known as the *phase problem*.[10] Fortunately, many methods have been developed to recover the phase profile. We focus here on three: error reduction (ER),[11,12] hybrid input-output (HIO),[13,14] and shrinkwrap.[15]

Iterative phase retrieval algorithms alternately project between the exit wave and diffraction pattern, applying certain constraints to the complex image in each space, as depicted in Fig. 3. These constraints are based on assumptions about the system and how it behaves. First, we assume that $\psi(\mathbf{r})$ and $\Psi(\mathbf{q})$ are related by Eq. (2), and so we can project our current "best guess" for the exit wave into the diffraction plane,

$$\Psi_n(\mathbf{q}) = \mathcal{F}[\psi_n(\mathbf{r})]. \tag{4}$$

Next, we assume that the measured intensity profile $I(\mathbf{q})$ is proportional to $|\Psi(\mathbf{q})|^2$ or, equivalently, that the two profiles have the same amplitude ($\sqrt{I(\mathbf{q})} = |\Psi(\mathbf{q})|$). We apply this relation as a constraint by multiplying the phase of our guessed diffraction pattern into the amplitude of our measurement,

$$\Psi'_n(\mathbf{q}) = \frac{\Psi_n(\mathbf{q})}{|\Psi_n(\mathbf{q})|}\sqrt{I(\mathbf{q})}. \tag{5}$$

The third step in the process is simply the inverse of Eq. (4), which returns an updated exit wave,

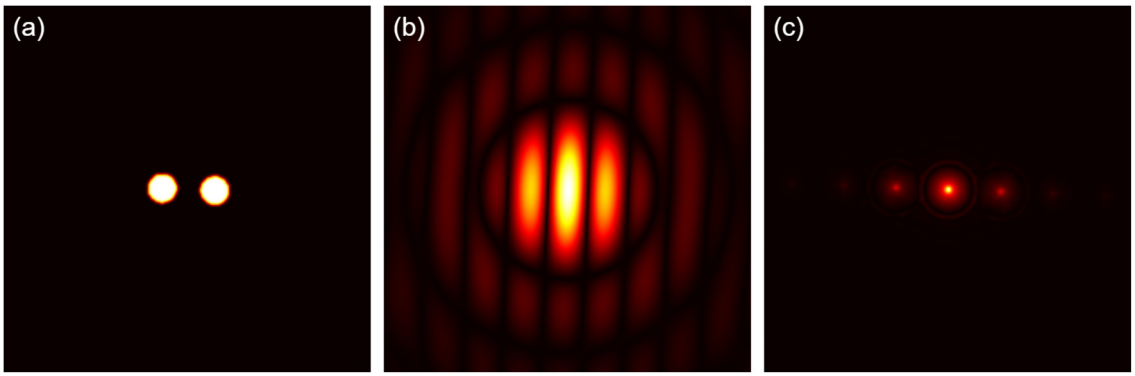

Fig. 2. (Color online) A simulated example of the phase problem, showing (a) a double-pinhole aperture, (b) the amplitude of its Fourier transform at the measurement plane, and (c) the amplitude of the inverse Fourier transform of (b). There are some basic features shared between (a) and (c), most notably a characteristic length between notable features. However, had the phase information been preserved, the two images would be identical. All three images have been cropped to a quarter of their original size in each dimension to show detail.

$$\psi'_n(\mathbf{r}) = \mathcal{F}^{-1}[\Psi'_n(\mathbf{q})]. \tag{6}$$

The final assumption is that $\psi(\mathbf{r})$ is nonzero only within some finite region $\mathbf{r} \in S$ (often called the "support region" or "support mask"), which is no larger than half of the overall reconstruction space in any direction.[16,17] The ER and HIO algorithms differ only in how they apply this constraint. In ER, it is applied quite directly,

$$\psi_{n+1}(\mathbf{r}) = \begin{cases} \psi'_n(\mathbf{r}), & \mathbf{r} \in S, \\ 0, & \mathbf{r} \notin S. \end{cases} \tag{7}$$

The ER method (as its name suggests) guarantees that the squared-error between $|\Psi_n(\mathbf{q})|^2$ and $I(\mathbf{q})$ is reduced on every iteration. However, it is vanishingly unlikely that a path exists from the initial guess to the correct answer that does not sometimes require increasing the error. For this reason, an iteration of HIO replaces Eq. (7) with

$$\psi_{n+1}(\mathbf{r}) = \begin{cases} \psi'_n(\mathbf{r}), & \mathbf{r} \in S, \\ \psi_n(\mathbf{r}) - \beta\psi'_n(\mathbf{r}), & \mathbf{r} \notin S, \end{cases} \tag{8}$$

where β is an adjustable parameter on the range $0 \leq \beta \leq 1$, typically 0.9. This modification allows a controlled amount of feedback to remain outside S, leading to a significantly more relaxed constraint that actually increases the squared-error, but still tends to improve $\psi_n(\mathbf{r})$ within S.

Shrinkwrap[15] is not a phase retrieval algorithm in itself, but rather a method of updating S to provide a stronger constraint for ER and HIO. The initial S generally allows many pixels to vary that should be set to zero, which leads to either stagnation or (at best) very slow convergence. However, as the rough shape of the aperture begins to appear, some of these incorrectly unmasked pixels can be easily identified as regions of very low amplitude. A common method of shrinkwrap is therefore to take a copy of the current direct space amplitudes, apply a Gaussian blur filter ($\sigma \sim 2$ pixels), then define the new S as all the pixels below a certain threshold relative to the maximum, thus "shrinkwrapping" the mask to the object.

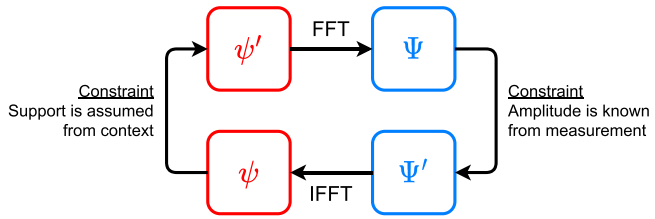

Fig. 3. (Color online) A flow chart depiction of iterative phase retrieval. The fast-Fourier transform (FFT) and inverse fast-Fourier transform (IFFT) are used respectively to project forward or backward between the two wave functions ψ and Ψ. In each space, constraints are applied based on known or assumed attributes of the wave field. Over many iterations, this process can recover the phase information lost during measurement.

There are some ambiguities that these methods cannot remove. The reconstructed aperture may appear anywhere in the direct space plane, including wrapped around the edges, since translation does not affect the magnitude of the Fourier transform. Similarly, the reconstructed image may appear upside down, though shrinkwrap (thankfully) breaks the symmetries that would otherwise allow for a superposition of the two flipped twin images.[15]

Still, these algorithms have proven to be highly robust when applied together and, despite their age, are still a staple of CDI experiments today. This is, in part, because of how they complement each other. In optimization terms, ER rapidly converges to a local minimum and stays there (much like a steepest descent method), HIO unstably seeks out a global minimum, and shrinkwrap reduces the search space, while also working as a stochastic element that can kick the reconstruction out of local minima and toward a global minimum.[18] One common phase retrieval "recipe" involves alternating ~100 iterations of HIO with ~10 iterations of ER, applying shrinkwrap after every iteration. In Sec. III B, we present a simple software package that allows students to play with this recipe to see how different number of iterations and parameters affect the reconstruction process.

C. Digital image processing

Up to this point, we have discussed diffraction mostly in idealized terms. Conducting an actual experiment introduces additional factors for which ideal models do not account. In a CDI experiment, many of these are related to digital imaging. Similar considerations appear in other forms of digital signal processing (DSP). Here, we will discuss three such principles—noise reduction, dynamic range, and

sampling—which, if not handled correctly, can make successful phase retrieval almost impossible.

Diffraction measurements typically exhibit two distinct types of noise, each requiring its own method of removal. The first type, sometimes called background, occurs when an unrelated/undesired signal is superimposed over the intended measurement. For example, light from a nearby window may fall on the detector while measuring a diffraction pattern. When such noise cannot be entirely eliminated at its source, it can instead be characterized and removed through background subtraction.

The second type of noise, Poisson noise, is a grainy quality that originates from the probabilistic nature of discrete photons and electrons. Background subtraction is not a viable option here, since the noise is randomized in each measurement based on a Poisson distribution.[19] The width of that distribution is proportional to the square root of the expected (i.e., noiseless) measurement. This also implies that the signal-to-noise ratio increases as the square root of signal. Since signal is proportional to integration period, the impact of Poisson noise can be reduced by increasing exposure time.

Dynamic range refers to the ratio between the largest and smallest values that can be measured in a single readout event or exposure of the image sensor. On a digital detector, this is equivalent to the total number of discrete values that can be output, and is typically represented in bits (b bits $= 2^b$ values). This can cause problems for CDI, because diffraction intensity often spans several orders of magnitude on a detector. If the detector does not have sufficient dynamic range, it will not be able to simultaneously measure the brightest and dimmest regions of a diffraction pattern; either the bright regions will saturate, or the dim regions will be dominated by noise. A detector's dynamic range can be artificially expanded by summing (or averaging) multiple measurements. The sum of N images taken on a b-bit detector with exposure time t is effectively the same as a single image taken with a $(b \log_2 N)$-bit detector with exposure time Nt.

In addition to discretizing intensities, a digital detector also divides an area into discrete pixels. In CDI, the size and resolution of the detector determine the size and resolution of the reconstruction through the Fourier diffraction model given in Eq. (2). For a detector with N pixels of size p_{det} (both measured along a single dimension), the reconstructed pixels would have size

$$p_{\text{rec}} = \frac{\lambda f}{N p_{\text{det}}} \tag{9}$$

along the same dimension. Noting that Np represents the total extent of an image, it becomes apparent that the extent of the detector determines the resolution of the reconstruction, and vice versa.

This is not an exhaustive list of possible issues that may affect a CDI experiment. Other factors may include Bayer filtering on an RGB detector,[20,21] etalon-like interference from a monochromatic beam passing through flat optics,[22] or nonlinear response from a detector near its saturation point.[23] Moreover, these specific principles are not universal to all possible experiments. However, identifying the unique limitations of an experiment is perhaps the most universally applicable learning outcome of any physics instructional laboratory.

III. MATERIALS

A. Apparatus

The low-cost and highly portable setup shown in Fig. 4 was developed as a way of maintaining the hands-on aspects of laboratory classes amid the widespread restrictions on in-person gatherings during 2020. Depending on the resources available to an instructor, the same apparatus can easily be assembled on an optical table with professional-grade equipment. An example of such an "upgraded" apparatus, as well as a list of the specific products used in both versions, is available as a supplementary material.

This experiment has five primary components—laser, beam expander, aperture, Fourier lens, detector—as shown in Fig. 4. The laser provides illumination. Any visible laser diode can work for this laboratory, although care should be taken to assure eye safety depending on the power level. The beam expander (two converging lenses separated by the sum of their focal lengths) ensures that the beam is wide and collimated. A custom aperture is placed in the expanded beam, producing a diffraction pattern that then passes through the Fourier lens (so named to distinguish it from lenses used in the beam expander). Finally, a detector is placed in the back focal plane of the Fourier lens (i.e., one focal length of the Fourier lens beyond the object).

Students may find the focal plane by minimizing the spot size formed by the laser on the detector. To avoid damage, however, the focused spot should not be left on the detector for an extended period. The distance from the aperture to the Fourier lens does not impact the scale of the diffraction features (Eqs. (3) and (9) have no z, only f). However, this distance *does* determine how spread out the diffraction pattern is when it passes through the lens. If a student finds that the

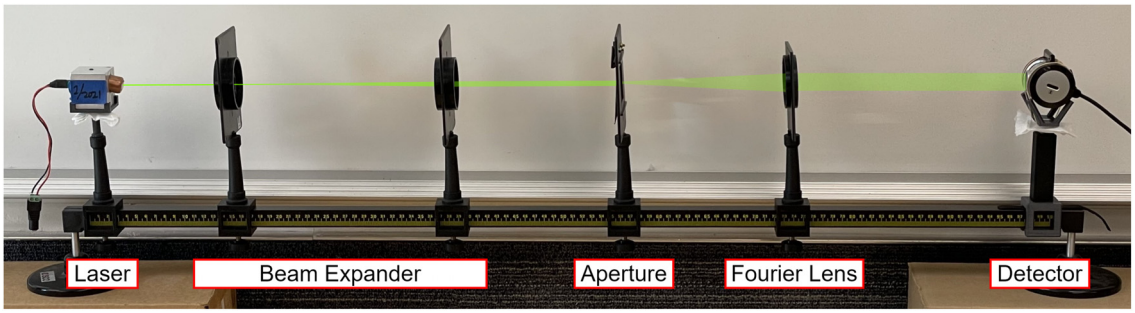

Fig. 4. (Color online) A low-cost, portable apparatus capable of performing CDI. The beam from a laser is broadened using a beam expander, then passed through an aperture and Fourier lens. At the focal plane of the lens, the light intensity profile is measured using a lensless camera. A green line representing the approximate path of the beam has been added to help with visualization.

diffraction pattern cuts off outside of a circular window, it is likely because the aperture is too far from the lens.

The detector can come from any digital camera, provided all lenses can be removed. If the pixel pitch (i.e., size) is not given in the camera specifications, it can often be found by searching "[camera model] image sensor" online. Failing this, it may be estimated by dividing the height or width of the detector by the number of pixels in that dimension. Similarly, if the bit depth (i.e., dynamic range) is not given, it can be found by examining the output values of a saturated image.

Students may make their own apertures out of any material that can block the laser while still being thin enough to pierce with a needle or scalpel. We recommend having students use a fine needle to punch holes in a piece of construction paper. Using Eq. (9) and the required dimensions of the support region S, one can show that the aperture must be contained within a square no larger than

$$L_{\max} = \frac{Np_{\text{rec}}}{2} = \frac{\lambda f}{2p_{\text{det}}} \tag{10}$$

on any given side. The pinholes may be in any arrangement within that region.

For the setup shown in Fig. 4, we used part of an Eisco Labs kit, which also included several lenses, two single-lens mounts, a flat sample mount, and several other components that are not needed for this experiment. At the time of writing, similar optics kits typically cost between US$100 and US$200. We also designed and 3D-printed some additional pieces compatible with the rail kit, including mounts for the laser, detector, and a third lens. Coherent light is provided by a 532 nm diode laser in an aluminum block with an angled IR filter mounted on the front (custom machined).

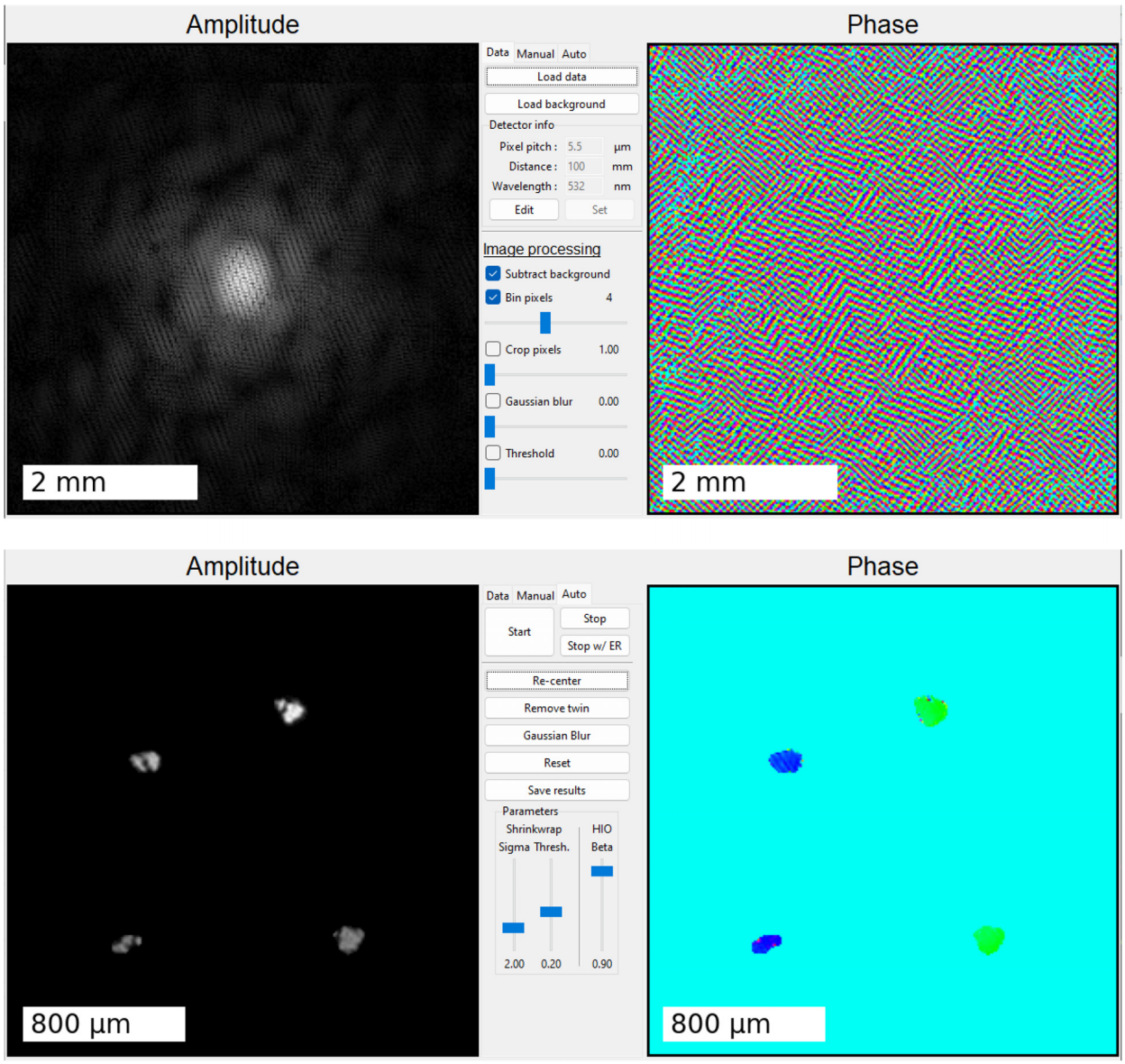

Fig. 5. (Color online) Screenshots of a reconstruction completed in the Interactive CDI application. The aperture consisted of four small holes in a sheet of construction paper. In the top screenshot, the diffraction (reciprocal space) amplitude and phase are displayed beside some image processing options. The reciprocal phase profile, initially randomized, takes on the intricate patterns seen here during reconstruction. In the bottom screenshot, the aperture (direct space) amplitude and phase are displayed beside the automatic reconstruction controls. Stray fibers from the paper, each approximately 20 μm in thickness, partially occlude the pinholes.

B. Software

The best image acquisition software for this experiment will vary depending on the image detectors being used. Many scientific detectors come with their own software, which provides straightforward access to many low-level imaging parameters. For nonscientific detectors (such as a webcam), this level of control may be more difficult to find. In general, however, any software that can lock the camera to a particular exposure time and analog gain level should be sufficient. Preferably, images should be saved in a lossless, uncompressed format such as TIFF.

For general image viewing and basic processing, we recommend the free and open-source software ImageJ.[24–26] For phase retrieval, we have developed an Interactive CDI application,[27] shown in Fig. 5. There are other phase retrieval applications that are more robust, optimized, and feature-rich than ours, though these are primarily focused on more advanced techniques such as Bragg CDI[28–32] or ptychography.[33–36] By contrast, our software was specifically designed as a first exposure to CDI. Both the compiled application and the Python source code are freely available online.[27]

IV. CONCLUSION

This experiment has been implemented as part of the advanced undergraduate physics instructional laboratory course (Physics 245 "Experiments in Contemporary Physics") at Brigham Young University. The course's laser optics unit spans eight three-hour classes, with the last two dedicated to CDI. Working in groups of two or three, our students generally find that two classes is sufficient time to obtain the two-pinhole image and begin exploring other avenues. Teaching only the CDI experiment without the rest of the unit would likely take a bit longer, since much of the apparatus (laser, aligning optics, beam expander, and detector) is set up during those first six days.

Depending on the time allotted to this unit and the desired learning outcomes, there are several possibilities for expansion. To build intuition with both diffraction and Fourier transforms, students may replace the double-pinhole with more complicated apertures, making observations on the relationship between the direct and reciprocal domains. For additional training in digital image processing, students may try to introduce, characterize, and digitally remove more complicated sources of noise (such as a dynamic external light source). Finally, for a much more in-depth study of phase retrieval or simply as a programming project, the Interactive CDI repository has a "do-it-yourself" branch with the same structure as the original, but with key phase retrieval functions left undefined.

As with the myriad other niche topics touched on in an undergraduate education, we recognize that it is unlikely that most students will pursue a career in CDI. However, this experiment uses knowledge applicable to many technical fields. By teaching these principles and skills through application, we hope to better prepare the next generation of physicists for a wide range of potential careers.

SUPPLEMENTARY MATERIAL

Please click on this link to access the supplementary material to assist instructors wishing to implement this lab. The first item, "Supplemental Document," contains additional details about the apparatus shown in Fig. 4, as well as an alternative apparatus that trades portability and low cost for stability and precision. The product number(s) of each component are tabulated. The second supplemental item, "Optics Mounts," is a compressed directory containing 3D-printable mounts used in the portable setup (Fig. 4). Print readers can see the supplementary material at https://doi.org/10.60893/figshare.ajp.c.7718444.

ACKNOWLEDGMENTS

This work was supported by the DOE Office of Science (Office of Basic Energy Sciences) (Award No. DE-SC0022133) and by the Department of Physics and Astronomy and College of Computational, Mathematical, and Physical Sciences at Brigham Young University.

AUTHOR DECLARATIONS

Conflict of Interest

The authors have no conflicts to disclose.

[a]ORCID: 0000-0002-8286-6179.
[b]ORCID: 0009-0009-0916-9842.
[c]ORCID: 0000-0001-6163-518X.
[d]ORCID: 0009-0002-2070-3451.
[e]ORCID: 0000-0001-9719-8188.

[1]G. Huldt, A. Szőke, and J. Hajdu, "Diffraction imaging of single particles and biomolecules," J. Struct. Biol. **144**, 219–227 (2003).
[2]S. Boutet and I. K. Robinson, "Coherent X-ray diffractive imaging of protein crystals," J. Synchrotron Rad. **15**(6), 576–583 (2008).
[3]M. A. Pfeifer, G. J. Williams, I. A. Vartanyants, R. Harder, and I. K. Robinson, "Threedimensional mapping of a deformation field inside a nanocrystal," Nature **442**(7098), 63–66 (2006).
[4]J. L. Jones, "The use of diffraction in the characterization of piezoelectric materials," J. Electroceram. **19**(1), 69–81 (2007).
[5]Michal Odstrčil, Andreas Menzel, and Manuel Guizar-Sicairos, "Iterative least-squares solver for generalized maximum-likelihood ptychography," Opt. Express **26**(3), 3108–3123 (2018).
[6]Michal Odstrčil, Mirko Holler, Jörg Raabe, and Manuel Guizar-Sicairos, "Alignment methods for nanotomography with deep subpixel accuracy," Opt. Express **27**(25), 36637–36652 (2019).
[7]I. A. Vartanyants, I. K. Robinson, J. D. Onken, M. A. Pfeifer, G. J. Williams, F. Pfeiffer, H. Metzger, Z. Zhong, and G. Bauer, "Coherent x-ray diffraction from quantum dots," Phys. Rev. B **71**(24), 245302 (2005).
[8]M. Ware and J. Peatross, *Physics of Light and Optics* (Brigham Young University, 2015).
[9]J. W. Goodman, *Introduction to Fourier Optics* (Roberts & Company Publishers, 2005).
[10]R. E. Burge, M. A. Fiddy, A. H. Greenaway, and G. Ross, "The phase problem," Proc. R. Soc., A **350**, 191–212 (1976).
[11]R. W. Gerchberg and W. O. Saxton, "A practical algorithm for the determination of phase from image and diffraction plane pictures," Optik **35**, 237–246 (1972).
[12]J. R. Fienup, "Reconstruction of an object from the modulus of its Fourier transform," Opt. Lett. **3**(1), 27–29 (1978).
[13]J. R. Fienup, "Iterative method applied to image reconstruction and to computer-generated holograms," Opt. Eng. **19**, 297–305 (1980).
[14]J. R. Fienup, "Phase retrieval algorithms: A comparison," Appl. Opt. **21**(15), 2758–2769 (1982).
[15]S. Marchesini, H. He, H. N. Chapman, S. P. Hau-Riege, A. Noy, M. R. Howells, U. Weierstall, and J. C. H. Spence, "X-ray image reconstruction from a diffraction pattern alone," Phys. Rev. B **68**(14), 140101 (2003).
[16]C. Shannon, "Communication in the presence of noise," Proc. IRE **37**, 10–21 (1949).
[17]D. Sayre, "Some implications of a theorem due to Shannon," Acta Cryst. **5**(6), 843–843 (1952).
[18]S. Marchesini, "A unified evaluation of iterative projection algorithms for phase retrieval," Rev. Sci. Instrum. **78**(1), 011301 (2007).

[19]G. Williams, M. Pfeifer, I. Vartanyants, and I. Robinson, "Effectiveness of iterative algorithms in recovering phase in the presence of noise," Acta Crystallogr., Sect. A **63**(1), 36–42 (2007).
[20]T. B. Jones, N. Otterstrom, J. Jackson, J. Archibald, and D. S. Durfee, "Laser wavelength metrology with color sensor chips," Opt. Express **23**(25), 32471–32840 (2015).
[21]T. T. Grove, C. Daly, and N. Jacobs, "Designer spectrographs for applications in the advanced undergraduate instructional lab," Am. J. Phys. **92**(3), 221–233 (2024).
[22]J. N. Porter, J. S. Jackson, D. S. Durfee, and R. L. Sandberg, "Laser wavelength metrology with low-finesse etalons and Bayer filters," Opt. Express **28**(25), 37788–37797 (2020).
[23]N. A. Riza, N. Ashraf, and M. Mazhar, "Optimizing the CMOS Sensor-Mode for Extreme Linear Dynamic Range MEMS-based CAOS Smart Camera Imaging," EPJ Web Conf. **238**, 12007 (2020).
[24]C. A. Schneider, W. S. Rasband, and K. W. Eliceiri, "NIH Image to ImageJ: 25 years of image analysis," Nat. Methods **9**(7), 671–675 (2012).
[25]J. Schindelin *et al*., "Fiji: an open-source platform for biological-image analysis," Nat. Methods **9**(7), 676–682 (2012).
[26]C. T. Rueden, J. Schindelin, M. C. Hiner, B. E. DeZonia, A. E. Walter, E. T. Arena, and K. W. Eliceiri, "ImageJ2: ImageJ for the next generation of scientific image data", arXiv:1701.05940 (2017).
[27]J. N. Porter, see https://github.com/jacione/interactivecdi for "Interactive CDI, GitHub repository" (2023).
[28]M. C. Newton, Y. Nishino, and I. K. Robinson, "Bonsu: the interactive phase retrieval suite," J. Appl. Crystallogr. **45**, 840–843 (2012).
[29]V. Favre-Nicolin, G. Girard, S. Leake, J. Carnis, Y. Chushkin, J. Kieffer, P. Paleo, and M.-I. Richard, "PyNX: high-performance computing toolkit for coherent X-ray imaging based on operators," J. Appl. Crystallogr. **53**(5), 1404–1413 (2020).
[30]S. Maddali (2020). "Phaser: Python-based BCDI phase retrieval for CPU and GPU," Zenodo. https://zenodo.org/record/4305131
[31]S. Maddali (2022). "MRBCDI: Differentiable, multi-reflection Bragg coherent diffraction imaging (BCDI) for lattice distortion fields in crystals," Zenodo. https://zenodo.org/record/6958797
[32]B. Frosik, R. Harder, and J. N. Porter, see https://github.com/AdvancedPhotonSource/cohere for "Cohere, GitHub repository" (2024).
[33]B. Enders and P. Thibault, "A computational framework for ptychographic reconstructions," Proc. R. Soc. A **472**, 20160640 (2016).
[34]Ondřej Mandula, Marta Elzo Aizarna, Joël Eymery, Manfred Burghammer, and Vincent Favre-Nicolin, "Ptycho: A computing library for X-ray coherent diffraction imaging of nanostructures," J. Appl. Crystallogr. **49**(5), 1842–1848 (2016).
[35]Z. Guan, E. H. Tsai, X. Huang, K. G. Yager, and H. Qin, "Ptychonet: Fast and high quality phase retrieval for ptychography," Report No. 1599580 [Brookhaven National Laboratory (BNL), Upton, NY, 2019].
[36]D. Gursoy and D. J. Ching, see https://doi.org/10.11578/dc.20230202 for "Tike, OSTI Archive" (2022).

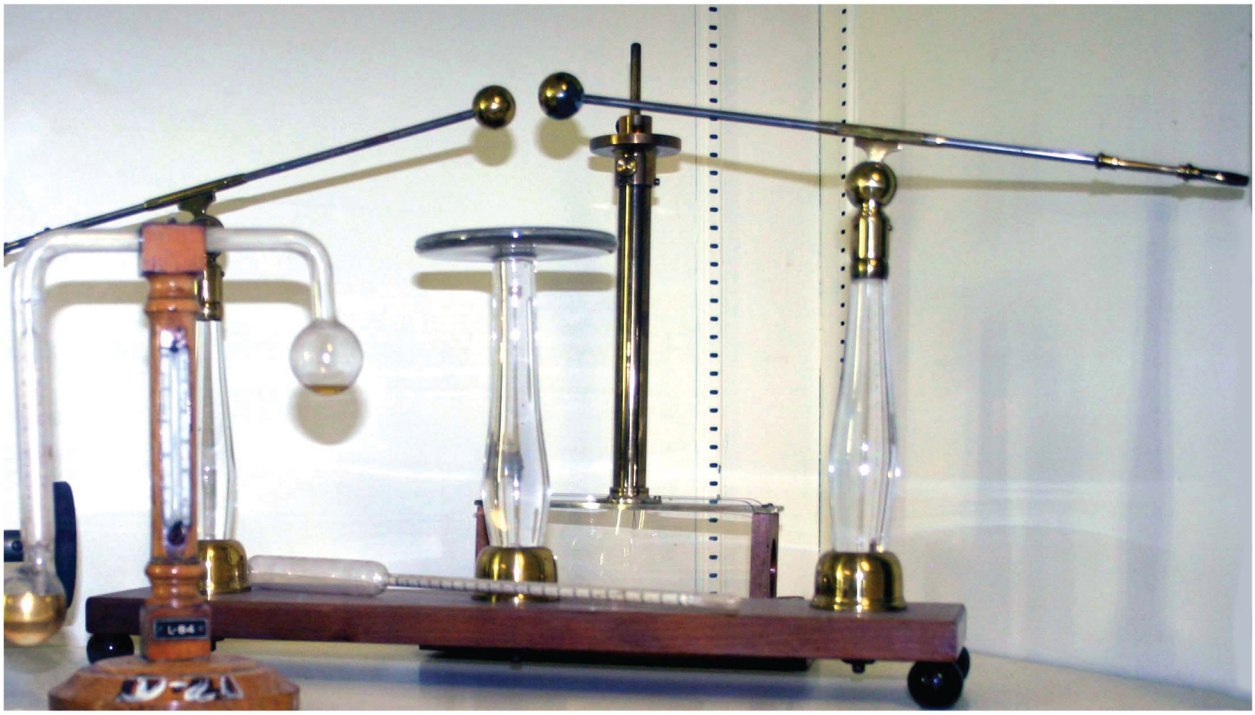

Universal Discharger

In the early part of the 19th century there was interest in seeing what would happen when a high voltage spark was passed through material, either organic (such as a frog's leg) or inorganic (firing gunpowder). The original instrument was developed by William Henley ca. 1770. The two electrodes are connected to an electrostatic machine, and the sample is placed atop the table. Sometimes a slab of ivory is let into the table top to serve as an insulator. This example was on display at the Rennselaer Polytechnic Instate when I passed by to give a talk in 2013. (Picture and text by Thomas B. Greenslade, Jr., Kenyon College)